Available online at www.sciencedirect.com
ScienceDirect
Journal of the European Ceramic Society 31 (2011) 121–127
www.elsevier.com/locate/jeurceramsoc

Cation order enhancement in Sr_2FeMoO_6 by water-saturated hydrogen reduction

Alberto Calleja [a,b,*], Xavier G. Capdevila [c], Mercè Segarra [c], Carles Frontera [a], Ferran Espiell [c]

[a] Institut de Ciència de Materials de Barcelona-Consejo Superior de Investigaciones Científicas, Campus de la UAB, 08193, Bellaterra, Spain
[b] Institut de Ciència i Tecnologia Ambientals, Universitat Autònoma de Barcelona, Campus de la UAB, 08193, Bellaterra, Spain
[c] DIOPMA, Departament de Ciència de Materials i Enginyeria Metal·lúrgica, Facultat de Química, Universitat de Barcelona, 08028, Barcelona, Spain

Received 22 January 2010; received in revised form 27 July 2010; accepted 2 August 2010
Available online 15 September 2010

Abstract

Sr_2FeMoO_6 (SFMO) double perovskite has been prepared from powders obtained by the polyacrylamide gel combustion synthesis. After removing organic residues, the precursor powder consists of a homogeneous submicronic blend of $SrFeO_{3-x}$ and $SrMoO_4$. In order to crystallize SFMO an experimental setup consisting of injecting water-saturated Ar/5%H_2 gas flow in a crucible was used. Results show that a high saturation magnetization of 3.9μ_B/formula unit, which accounts for 98% of the theoretical value, and Curie temperature of 415 K can be achieved in this way. The Fe/Mo order was 98% by Rietveld refinement of best sample. Furthermore, no metallic iron was detected, even at long reducing treatments. Lowering the reducing power of hydrogen with water is believed to be the main reason for improved synthesis.

Keywords: A. Sol–gel processes; B. Microstructure-final; C. Magnetic properties; D. Perovskites; SFMO

1. Introduction

Transition-metal oxide double perovskites of the type $A_2B'B''O_6$ where A = Ca, Sr, Ba and B′,B″ = Fe, Cr, Ni, Mo, Re or W have potential applications in the field of spintronics,[1] gas sensors,[2] magnetic sensors,[3,4] magnetocaloric materials[5] and, more recently, anodes for solid-oxide fuel cells.[6] The B′ and B″ ions should be alternatively arranged along the cubic axes of the double perovskite. The presence of antisite defects (AS) in the B-site due to imperfect alternation leads to reduced magnetization and electronic polarization. A topical review on double perovskites by Serrate et al. has been published elsewhere.[7]

Since the discovery of low-field magnetoresistance at high temperatures in half-metal Sr_2FeMoO_6 (SFMO),[8] the double perovskite is being studied for spintronic devices exploiting magnetic tunnel junctions (MTJ)[9,10,11] or contact-less potentiometric sensors for the automotive industry.[12] These applications are enabled by the high spin polarization of the conduction band. In principle, its high Curie temperature (T_C = 415 K) makes it more promising than colossal magnetoresistance manganites like $La_{2/3}Sr_{1/3}MnO_3$ with T_C = 350 K. The ionic representation of the crystal lattice shows Fe^{3+} ($3d^5$, S = 5/2) and Mo^{5+} ($4d^1$, S = 1/2) sublattices coupled antiferromagnetically between them. Half-metallicity arises from the itinerant $4d^1$ electron in the Mo^{5+} ion. AS defects dramatically influence spin polarization and saturation magnetization.[13] Magnetotransport is thus a function of AS concentration, grain boundaries and crystallite size. Magnetoresistance values as high as 31% at room temperature have been reported in high aspect ratio SFMO crystals.[14]

Most of the synthesis procedures in the literature make use of the solid-state reaction for producing bulk powders.[15] Phase evolution by powder X-ray diffraction gives insight into the formation kinetics.[16] SFMO growth from the two-phase mixture composed of perovskite $SrFeO_{3-x}$ (SFO) and $SrMoO_4$ (SMO) has been previously investigated. Basically, SMO would diffuse towards SFO during the reduction step at high temperature to form the solid solution compound $Sr_2Fe_{2-x}Mo_xO_y$. In fact, SFO shows similar structure to SFMO. Shift of SFO X-ray diffraction peaks as reaction proceeds would point to molybdenum solution in the SFO lattice. Redox issues have to be also considered as Mo

* Corresponding author at: Institut de Ciència de Materials de Barcelona-Consejo Superior de Investigaciones Científicas, Campus de la UAB, 08193, Bellaterra, Spain. Tel.: +34 935801853; fax: +34 935805729.
E-mail address: acalleja@icmab.es (A. Calleja).

0955-2219/$ – see front matter © 2010 Elsevier Ltd. All rights reserved.
doi:10.1016/j.jeurceramsoc.2010.08.002

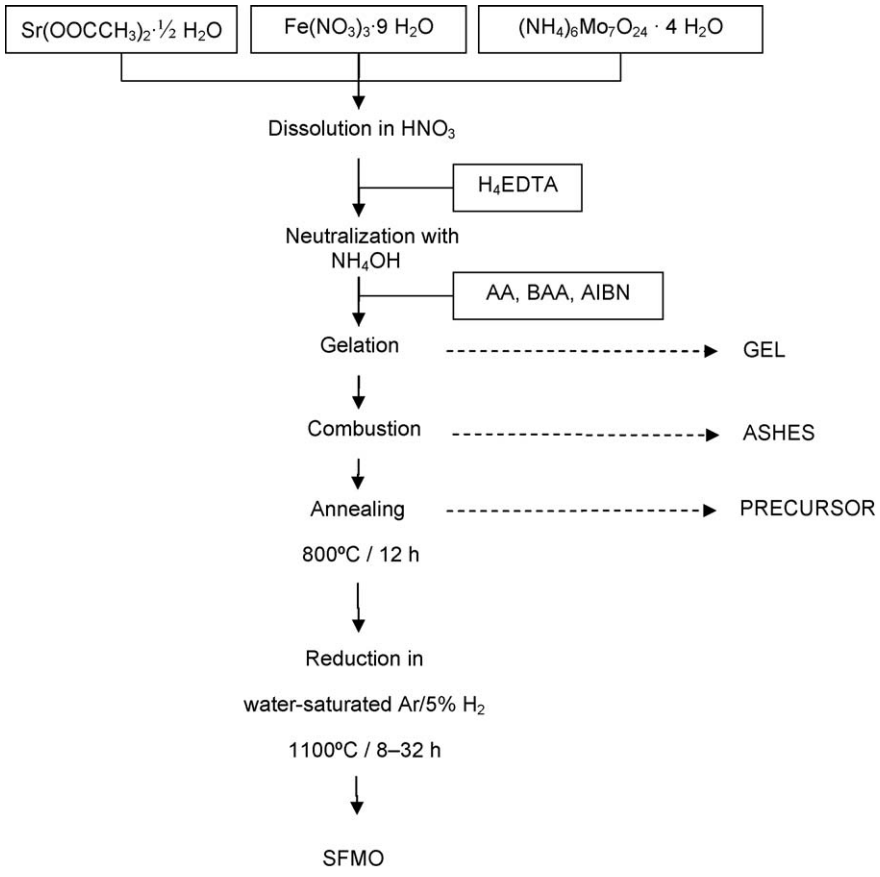

Fig. 1. Flowchart of the synthesis procedure. AA, BAA and AIBN stand for acrylamide, bisacrylamide and azoisobutyrnitrile, respectively.

is in a 6+ oxydation state in SMO while is 5+ in SFMO. Sharma et al.[17] have determined the phase stability of SFMO as a function of oxygen partial pressure P_{O_2} in a H_2/CO_2 atmosphere and MacManus-Driscoll et al.[18] observed molybdenum enrichment in the SFMO grain boundary when studying the effect of cyclic oxygenation on low-field magnetoresistance.

One of the main problems during synthesis is the excessive reduction producing Fe^{2+} species and even metallic iron, before SFMO reaction completion, which can artificially increase saturation magnetization.[19] Another concern is phase stability at ambient conditions. Both Fe^{2+} and Mo^{5+} have been shown to slowly oxidize in air in the long term.[20,21] Notoriously, the use of citric acid with nitrate salts has enabled the obtention of top quality SFMO powders with $3.9\mu_B$/f.u. saturation magnetization and a high T_C of 416 K.[22] The quartz tube encapsulation technique has been successfully used by Huang et al.[19] starting from a EDTA gel. Pechini-like methods have also been explored.[23] Furthermore, epitaxial thin films have been prepared by pulsed-laser deposition[24] and chemical solution approaches.[25] In general, synthesis conditions have to be carefully tuned for preparing pure double perovskite with small AS concentration during the reducing step as evidenced by deviation from the theoretical saturation magnetization at low temperature ($4.0\mu_B$/f.u.).[26]

From the synthesis viewpoint, polymer gel combustion has been shown to render nanometric electroceramic powders with excellent chemical and phase purities by employing long-chain soluble polymers by acrylamide monomer polymerization or dissolved poly(vinylalcohol).[27,28] However, obtaining pure phases with a high degree of superstructure also remains a challenging issue for these kind of techniques.

In this work, the acrylamide gel polymerization technique was used to produce SFMO precursor powders. Then, SFMO formation was achieved by means of a reducing step at high temperatures involving water-saturation of the inlet gas. It is shown that high yield of SFMO with excellent alternate Fe/Mo ordering can be obtained minimizing the formation of undesired reduced species leading to 98% of theoretical saturation magnetization and a high Curie temperature of 415 K.

2. Experimental

A flowchart showing the general synthesis scheme is shown in Fig. 1.

Aqueous metal salt solution starts by weighting stoichiometric amounts of $Sr(OOCCH_3)_2{\cdot}½H_2O$ 99.5%, $(NH_4)_6Mo_7O_{24}{\cdot}4H_2O$ 99.9% and $Fe(NO_3)_3{\cdot}9H_2O$ 99.99% (Quality Chemicals). pH adjustment is done between 3.5 and 5.5 with either diluted nitric acid or ammonia. Acrylamide monomer is poured in the form of a 50% aqueous solution (Cognis) in a concentration of 10% w/v with respect to monomer. In order to avoid the acrylamide polymerization inhibition

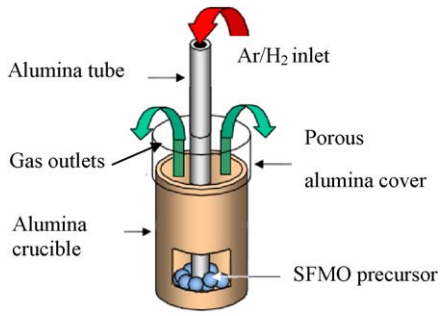

Fig. 2. Experimental setup of the gas flow injection in the alumina crucible.

from the Fe^{3+} or Mo^{6+} species, ethylenediaminetetraacetic acid (H_4EDTA) is added to complex metals. Bisacrylamide (Alfa Aesar) in 1/8 weight ratio with respect to acrylamide is added to effect crosslinking and azoisobutyronitrile (Alfa Aesar) as a radical initiator. Before gelation, total metal cation concentration (Sr, Fe and Mo) is 0.17 M. Gel formation by polymerization is achieved by heating the solution at 80 °C by means of a hot plate. SFMO gel is removed from the glass beaker and placed in a more resistant stainless steel container. Once gel has been combusted in air with the aid of a hot plate set at 300 °C to start the process, the ashes are placed in a vitrified porcelain cup and annealed at 800 °C to remove organic impurities from partial decomposition of the polymer. Then the precursor powder was pressed into 1-in. round pellets in steel dies applying a uniaxial pressure of 2000 bar.

The reduction step for obtaining SFMO, comprises Ar/H_2 5% gas injection in an 99.7% alumina cylindrical crucible. Inner diameter and height of the crucible was 20 mm and 40 mm, respectively. Gas is saturated with water by means of a gas washer bottle and then driven to the bottom of the crucible with an alumina tube having a inner diameter of 8 mm. Chunks of the SFMO precursor pellet are placed inside the crucible and around the inlet tube. The gas exits through a loose lid made of refractory alumina brick. Gas flow was varied between 0.14 and 0.70 l/min. This setup allowed the SFMO preparation in quantities around 50 g. See Fig. 2 for a general scheme. The precursor pellet was manually crushed into approximately 5 mm chunks. The heating ramp was 15 °C/min and furnace cooling was applied after soaking.

Carbon and nitrogen impurities were measured by elemental analysis with a ANALYTICAL PRECISION model EA1108. XRD diffraction was performed in a Siemens D500 with CuKα radiation. Powder X-ray data has been analyzed by the Rietveld method using FullProf suite of programs.[29] Maximum intensity peak in each pattern was assigned 100% and then the maximum diffraction peak of each phase was calculated as a percentage. Scanning electron microscopy was performed in a Hitachi 2300 model. Transmission electron microscopy of the powder was performed in a Hitachi 600AB. Magnetization loops were determined at different temperatures by means of a Quantum Design SQUID magnetometer. Saturation magnetization value was obtained at 10 K and 50 kOe.

3. Results and discussion

A spongy mass is obtained due to the large amount of decomposition gases being released during combustion through the viscous gel mass. Elemental analysis of SFMO ashes results in $1.99 \pm 0.01\%$ and $0.34 \pm 0.02\%$ of carbon and nitrogen impurities in the ashes, respectively. The high carbon value could be explained by the partial carbonation of the oxides. In fact, reflections corresponding to $SrCO_3$ are clearly identified by X-ray diffraction (Fig. 3). Nitrogen impurities would point to incomplete combustion of the polyacrylamide. The rest of the XRD peaks correspond to $SrMoO_4$. Scherrer's formula applied to the highest intensity peak (1 1 2) of this phase gives a crystallite size of 39 nm. Iron-containing phases do not appear. It is thought that crystallization has not been promoted for the expected $SrFeO_{3-x}$ (SFO) phase during the short self-combustion time. Moreover, an important fraction of strontium is in the carbonate form, which further prevents the existence of the binary iron compound. In this respect, no iron oxides are detected by XRD, which might be due to their low crystallinity.

Before crystallization process in reducing conditions, decarbonation of the ashes seems advisable, specially if organic residues remain which could eventually form stable carbonaceous species and hamper crystal growth of the double perovskite.

A thermal treatment at 800 °C for 12 h is able to remove most of the organic impurities while avoiding excessive grain coarsening, which would result in longer diffusion paths and reduced reactivity for the $SrFeO_{3-x}$ and $SrMoO_4$ particles to contact and form SFMO. Carbon is reduced to $0.28 \pm 0.02\%$ while nitrogen is no longer detected. XRD pattern of the so-called SFMO precursor powders is plotted in Fig. 4. Only peaks corresponding to SFO and SMO are visible. In addition, SFO peaks appear wider than SMO. This may be due to insufficient SFO crystallization at the present annealing conditions. The main SFO reflection peak is at 32.5° which is in accordance with $SrFeO_{3-x}$ in equilibrium at these conditions.[30] Interestingly, no $SrCO_3$ peaks were identified, indicating that decarbonation has been achieved within XRD resolution limits. SEM corresponding to the precursor is

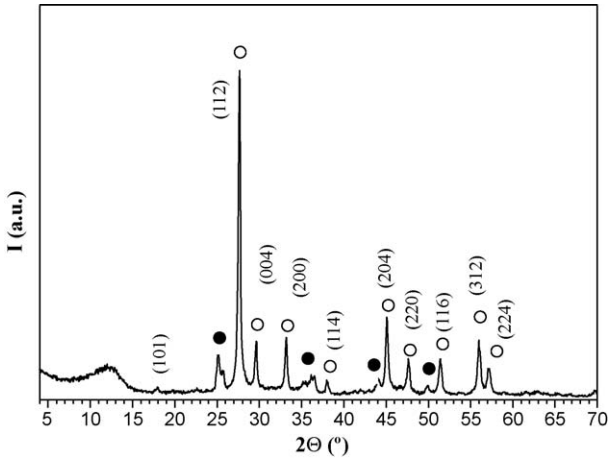

Fig. 3. XRD pattern of the ashes obtained after gel combustion. (●) and (○) symbols stand for $SrCO_3$ and $SrMoO_4$, respectively.

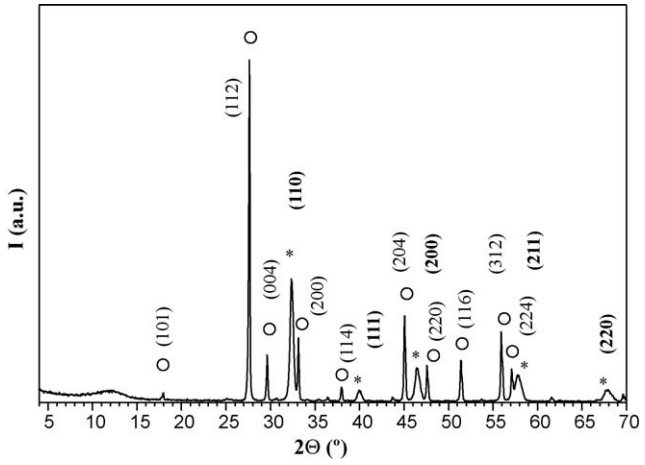

Fig. 4. XRD of SFMO precursor powder, once calcined at 800 °C/12 h in air. (◯) and (*) symbols stand for $SrMoO_4$ and $SrFeO_{3-x}$, respectively. Miller indexes in bold correspond to $SrFeO_{3-x}$.

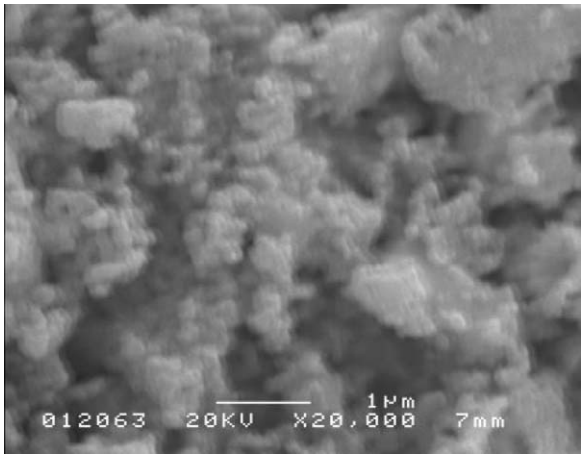

Fig. 5. SEM micrograph of SFMO precursor powder.

shown in Fig. 5. It is composed of low-density aggregates in which SFO and SMO particles cannot be distinguished from one another. Particles size of the agglomerates are below 1 μm. Hence, the polymer gel precursor is a submicronic two-phase solid mixture of seggregated iron and molybdenum species.

Starting from this precursor SFMO powders, first attempts to grow SFMO in Ar/5%H_2 were not successful if loose powders were used. However, after pressing the precursor, reaction could be observed. This is a hint of the relevance of solid diffusion during the heterogeneous reaction of SFMO formation.

In the reduction step, gas flow is injected directly towards the pressed precursor in order to increase mass transfer in the gas phase during the SFMO formation. An important modification involves the saturation of the inlet gas with water at ambient temperature. Water is used as a means to diminish the reducing power of gases in typical metallurgical process, based on the decomposition equilibrium of H_2O at high temperatures ($H_2O \leftrightarrow H_2 + ½O_2$). In fact, by using thermochemical graphical tools like the Ellingham's diagram[31] and assuming water saturation of the Ar/5%H_2 process gas at 25 °C is fulfilled, which gives a water partial vapour pressure of $P_{H_2O} = 3.2 \cdot 10^{-2}$ atm and a hydrogen partial pressure of $P_{H_2} = 0.05$ atm, the P_{O_2} is 10^{-14} atm or 7 orders of magnitude higher than without water-saturation. In this way, oxygen partial pressure (P_{O_2}) can be increased while still being able to reduce the precursor as will be shown below. 1100 °C was chosen as the reducing temperature. Different synthesis conditions by changing gas flow, SFMO precursor initial mass and soaking time were investigated. It is believed that gas flow changes the dynamics of the gas-solid interface, impacting on the kinetics of the heterogeneous reaction. On the other hand, initial mass is thought to be important for the overall gas concentration. Finally, soaking time allows to explore the kinetics of the process. Table 1 lists the results of the samples prepared with such procedure. Note that M_{sat} is as high as 3.4μ_B/f.u. in just 8 h. X-ray diffraction pattern containing Rietveld refinement of the best sample is shown in Fig. 6. As found in the literature, the cell is tetragonal with space group *I 4/m* (no. 87). The refinement rendered very good agreement parameters ($\chi^2 = 3.8$; $R_B = 1.89\%$) whereas cell parameters agree well with those previously reported for this compound: $a = 5.5673(5)$ Å and $c = 7.8999(7)$ Å. The good contrast between Fe (Z = 26) and Mo (Z = 42) allows the precise determination of the degree of order between these two species located at *2a* and *2b* Wyckoff positions of *I 4/m* space group. The degree of Fe/Mo order obtained by the refinement is 98%, expressed as 2(g_{Fe}-0.5) where g_{Fe} is the Fe occupancy in its expected site. Powder data reveals the presence of a small amount of $SrMoO_4$ as an impurity. The quantitative analysis through the Rietveld refinements shows that the amount of this impurity is smaller than 1.5% (w/w).

An alternative indication of the Fe/Mo ordering in SFMO was reported by Balcells et al.,[15] which consists of calculating the intensity ratio $I(1\,0\,1)/(I(1\,1\,2) + I(2\,0\,0))$ from the XRD peaks.

Table 1
Results of SFMO precursor reduced by water-saturated Ar/5% H_2 flow.

Sample	Precursor mass (g)	Thermal treatment	Gas flow (l/min)	%XRD intensity SFMO	%XRD intensity $SrMoO_4$	M_{sat} (μ_B/f.u.)	%Theoretical M_{sat}
1	0.7	1100 °C/8 h	0.42	100	2	3.4	85%
2	1.0	1100 °C/16 h	0.42	100	6	3.3	83%
3	13.0	1100 °C/16 h	0.42	100	11	3.1	78%
4	16.3	1100 °C/24 h	0.42	100	10	3.1	78%
5	50.0	1100 °C/24 h	0.42	100	5	3.6	90%
6	23.0	1100 °C/24 h	0.70	100	6	3.9	98%
7	1.5	1100 °C/32 h	0.70	100	4	3.4	85%
8	0.5	1100 °C/32 h	0.70	100	1	3.9	98%

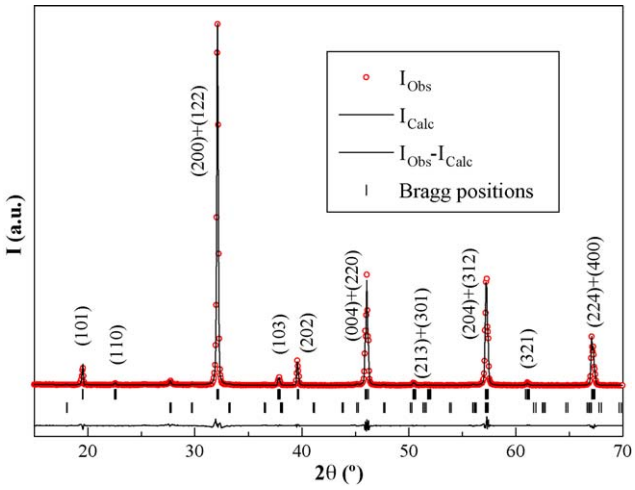

Fig. 6. Rietveld refinement of XRD pattern corresponding to sample 8 showing both high compositional purity and cation order. Marks below the pattern represent the reflections for Sr_2FeMoO_6 and binary $SrMoO_4$.

In our case, this value gives 0.05(2), which is coherent with the observed high saturation magnetization.

Remarkably, no metallic iron or Fe(II) phases are observed in any of the experiments. As a consequence, water-saturation has proved to be effective in avoiding excessive reduction. Accordingly, neither $SrMoO_3$[32] nor $Sr_3Fe_{2-x}Mo_xO_6$[33] appears. This is true even at long treatment times. Second, gas flow higher than 0.42 l/min is needed for obtaining high saturation magnetization. Best values were achieved with 0.70 l/min and 32 h. On the other hand, maximum M_{sat} of 3.9μ_B/f.u. was obtained at this gas flow value with two different initial mass/dwell time combinations (see samples 6 and 8). The fact that as much as 50 g can be prepared in a single run with M_{sat} as high a 3.6μ_B/f.u., i.e., 90% of theoretical value is also highlighted.

SEM micrograph with different magnifications corresponding to the sample no. 8 are shown in Fig. 7. Polycrystalline aggregates of faceted SFMO grains around 1 μm size are observed. Particles are partially sintered. As regards TEM, the observations made on the same sample are shown in Fig. 8. The SFMO grains are surrounded by smaller attached particles. This granular structure can be better observed at higher magnifications, where isometric particles with a size around 50 nm are well visible at the border of the large SFMO grains. These smaller grains might be the SMO secondary phase (visible in XRD), although phase identification should be undertaken together with some aging studies to elucidate whether its origin is incomplete reduction or surface degradation due to Mo^{+5} oxidation in air after the synthesis process. Anyway, this shows that SFMO grain boundaries are far from being free from impurities. This should have enormous impact on the low-field magnetoresistance.

Magnetic characterization data for the 8 sample is shown in Fig. 9. M_{sat} was as high as 3.9μ_B/f.u. or 98% of theoretical M_{sat} whereas temperature-dependence of the magnetization results in a Curie temperature of 415 K, which is among best values reported in the literature (410–420 K).[34]

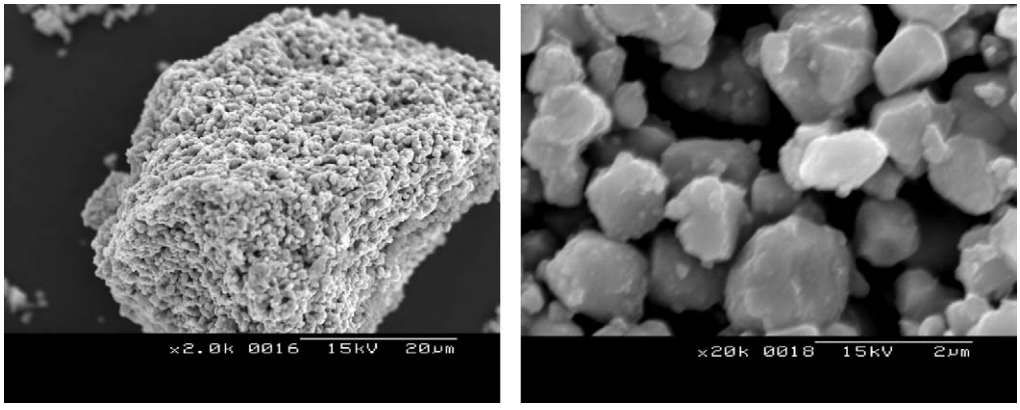

Fig. 7. SEM micrographs showing the SFMO aggregates and primary particles.

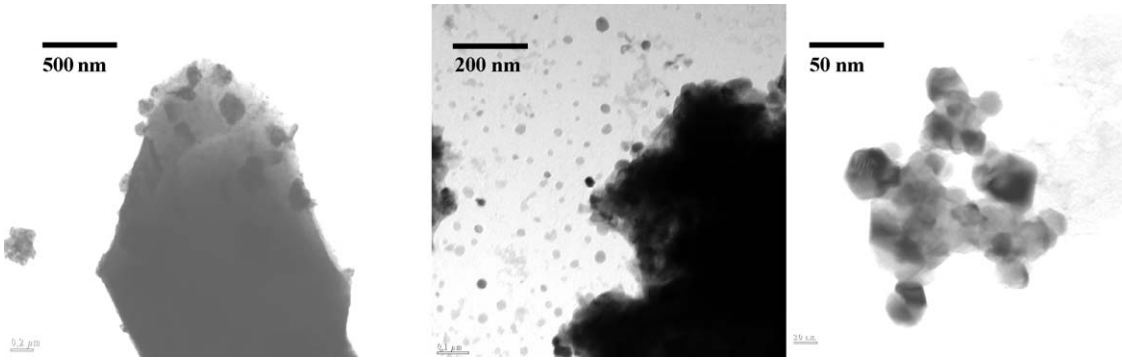

Fig. 8. TEM images of sample 8 at increasing magnifications.

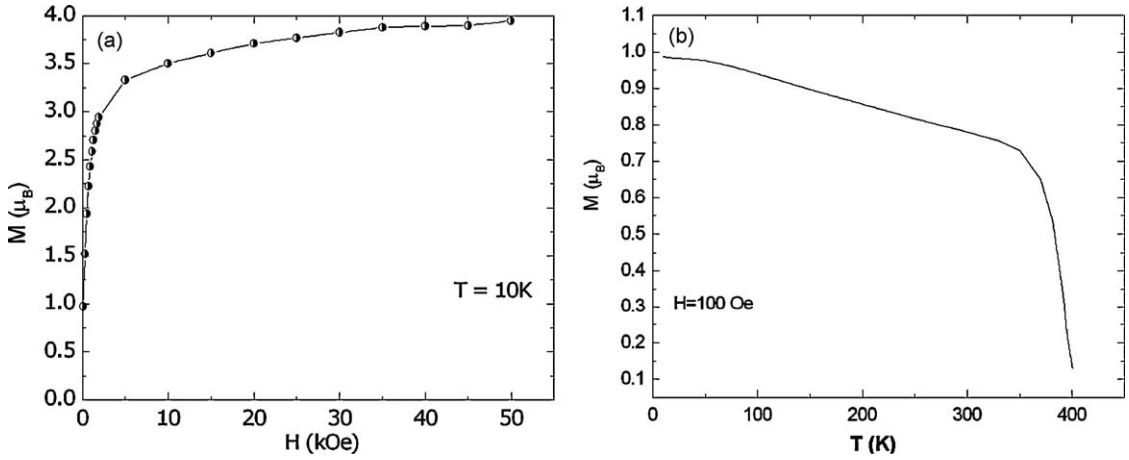

Fig. 9. (a) Magnetization curve at 10 K up to H = 50 kOe, in which M_{sat} reaches 3.9μ_B/f.u. (b) Temperature dependence of the magnetization at 100 Oe of sample 8 showing a T_C value of 415 K (extrapolated).

Table 2
Comparison of the results obtained in this work with respect to other SFMO synthesis.

Precursors	Gas composition	Thermal treatment	%Fe/Mo order by Rietveld analysis	M_{sat} (μ_B/f.u.)	T_C (K)	Impurities detected by XRD	Reference
Prereacted SFMO	H_2/CO_2	1300 °C/5 24 h	>95%	3.70	N/A	$SrCO_3$, $SrMoO_4$, Sr_3MoO_6	17
EDTA gel	Vacuum	1150 °C/100 h	95%	3.96	406	None reported	19
Citrate gel	Ar/1%H_2	1200 °C/12 h	94%	3.97	416	None reported	22
$Sr_2FeO_{3.5} + MoO_3$	N_2/5%H_2	1100 °C/2 h	95%[a]	3.7	N/A	$SrMoO_4$, Fe	23
Solid-state reaction	Ar/H_2/CO_2	1100 °C/6 h	82%[b]	3.0	N/A	None reported	35
Polyacrylamide gel	Ar/5%H_2	1100 °C/32 h	98%	3.9	410	$SrMoO_4$	This work

[a] Derived from $I(1\,0\,1)/(I(1\,1\,2) + I(2\,0\,0))$ XRD ratio.
[b] Derived from M_{sat}.

Table 2 summarizes some relevant reports in the literature about SFMO synthesis as regards reducing conditions. Concerning the Fe/Mo order, values higher than 90% have been reported with a variety of precursor preparations, atmosphere compositions, temperatures and dwell times. A common trend of using hydrogen diluted in inert gases is the appearance of metallic iron when higher temperatures and long reducing times have been applied, which suggests that pure SFMO synthesis is governed by kinetic control in these cases. Remarkably, metallic iron could be avoided when a mixture of hydrogen and carbon dioxide was used, increasing P_{O_2} and thus lowering the reducing power of the atmosphere, leading to high cation order and saturation magnetization.[17] However, CO_2 poses the problem of $SrCO_3$ formation, which is stable at these conditions, adversely influencing the double perovskite synthesis. By using water vapour in hydrogen gas as another approach to increase P_{O_2} and avoiding strongly reduced species like metallic iron, preparing SFMO with high cation order (98%) and saturation magnetization is also possible. However, the present results cannot rule out kinetic control of the synthesis, despite being able to reduce the precursor at 1100 °C for a long period like 32 h without Fe^0. That would require a more detailed study to gain insight into the phase diagram in this atmosphere composition. In fact, some SMO impurity still remains in the best sample and probably some unidentified iron-rich SFO phase, which is necessary for stoichiometric compensation of the molybdenum-rich SMO. In addition, there is no simple correlation between Fe/Mo order and M_{sat} which would point to some fraction of the observed magnetic moment originating from phases other than SFMO.

4. Conclusions

SFMO formation from polymer gel precursor powders was studied. After removing organic residues, the precursor is composed of a two-phase solid mixture of $SrMoO_4$ and $SrFeO_{3-x}$. The reducing step was performed by using water-saturated Ar/5%H_2 gas flow injected in a crucible at 1100 °C. Diminishing the reducing power of hydrogen by water saturation of the inlet gas was proved to be effective in obtaining cation ordered SFMO in high yield showing 98% of theoretical saturation magnetization at 10 K while preventing reduced phases like magnetic metallic iron, even at longer times of 32 h. Thus, water-saturated Ar/H_2 gas might be useful to obtain high cation ordered SFMO, although some minor phases like SMO still persist. This study also reveals the importance of the gas flow conditions as a limiting step in the SFMO crystallization from the precursor phases, which should be properly enhanced for optimum mass transfer.

Acknowledgements

The authors wish to thank Ministerio de Educación y Ciencia for the project Digital Magnetoresistive Oxide Sensors

(DIMOS) and Serveis Científico-Tècnics de la Universitat de Barcelona. Prof. J. Fontcuberta is greatly acknowledged for the magnetic measurements and helpful discussions. We are also grateful to XaRMAE from Generalitat de Catalunya. A.C. thanks Ministerio de Ciencia e Innovación for the Spanish Ramón y Cajal program.

References

1. Bibes M, Barthélémy A. Oxide spintronics. *IEEE Trans Electron Devices* 2007;**54**:1003–23.
2. Chaudhari GN, Gedam NN, Jagtap SV, Manorama SV. H_2S sensing properties of nanocrystalline $Sr_2Fe_{0.6}Ni_{0.4}MoO_6$ thick film prepared by sol–gel citrate method. *Talanta* 2009;**77**:1675–9.
3. Stoeffler D. First principle study of the electronic structure of $Sr_2FeMoO_6/SrTiO_3$ multilayers with and without interfacial Fe deficiency. *Eur Phys J B* 2008;**62**:19–25.
4. Fix T, Da Costa V, Ulhaq-Bouillet C, Colis S, Dinia A, Bouzehouane K, et al. High quality $SrTiO_3$ tunnel barrier obtained by pulsed laser deposition. *Appl Phys Lett* 2007;**91**:083104.
5. Zhong W, Tang NJ, Liu XL, Liu W, Chen W, Jiang HY, et al. Magnetocaloric effect above room temperature in the ordered double-perovskite $Ba_2Fe_{1+x}Mo_{1-x}O_6$. *J Magn Magn Mater* 2004;**282**:151–5.
6. Wei T, Chi Y, Meng X, Zhang Y. $Sr_2NiMoO_{6-\delta}$ as anode material for $LaGaO_3$-based solid oxide fuel cell. *Electrochem Commun* 2008;**10**:1369–72.
7. Serrate D, De Teresa JM, Ibarra MR. Double perovskites with ferromagnetism above room temperature. *J Phys: Condens Matter* 2007;**19**:023201.
8. Kobayashi KI, Kimura T, Sawada H, Terakura K, Tokura Y. Room-temperature magnetoresistance in an oxide material with an ordered double-perovskite structure. *Nature* 1998;**395**:677–80.
9. Bibes M, Bouzehouane K, Barthélémy A, Besse M, Fusil S, Bowen M, et al. Tunnel magnetoresistance in nanojunctions based on Sr_2FeMoO_6. *Appl Phys Lett* 2003;**83**:2629–31.
10. Fix T, Versini G, Loison JF, Colis S, Schmerber G, Pourroy G, et al. Pressure effect on the magnetization of Sr_2FeMoO_6 thin films grown by pulsed laser deposition. *J Appl Phys* 2005;**97**:024907.
11. Fix T, Stoeffler D, Henry Y, Colis S, Dinia A, Dimopoulos T, et al. Diode effect in all-oxide Sr_2FeMoO_6-based magnetic tunnel junctions. *J Appl Phys* 2006;**99**:08J107.
12. Fontcuberta J, Forniés C, Calleja A, Rubí D, Martínez B, Lacaba M, et al. Magnetoresistive ceramics, recent progress: from basic understanding to applications. *Bol Soc Esp Ceram Vidr* 2004;**43**:627–33.
13. García-Hernández M, Martínez JL, Martínez-Lope MJ, Casais MT, Alonso JA. Finding universal correlations between cationic disorder and low field magnetoresistance in FeMo double perovskite series. *Phys Rev Lett* 2001;**86**:2443–6.
14. Zhong W, Tang NJ, Au CT, Du YW. Bulrush-like double perovskite: synthesis, tunneling magnetoresistance and magnetocaloric effects. *J Nanosci Nanotechnol* 2008;**8**:2793–810.
15. Balcells Ll, Navarro J, Bibes M, Roig A, Martinez B, Fontcuberta J. Cationic ordering control of magnetization in Sr_2FeMoO_6 double perovskite. *Appl Phys Lett* 2001;**78**:781–3.
16. Fang TT, Wu MS, Ko TF. On the formation of double perovskite Sr_2FeMoO_6. *J Mater Sci Lett* 2001;**20**:1609–10.
17. Sharma A, MacManus-Driscoll JL, Branford W, Bugoslavsky Y, Cohen LF, Rager J. Phase stability and optimum oxygenation conditions for Sr_2FeMoO_6 formation. *Appl Phys Lett* 2005;**87**:112505.
18. MacManus-Driscoll JL, Sharma A, Bugoslavsky Y, Branford W, Cohen LF, Wei M. Reversible low-field magnetoresistance in $Sr_2Fe_{2-x}Mo_xO_{6-\delta}$ by oxygen cycling and the role of excess Mo ($x > 1$) in grain-boundary regions. *Adv Mater* 2006;**18**:900–4.
19. Huang YH, Linden J, Yamauchi H, Karpinnen M. Simple and efficient route to prepare homogeneous samples of Sr_2FeMoO_6 with a high degree of Fe/Mo order. *Chem Mater* 2004;**16**:4337–42.
20. Kuepper K, Raekers M, Taubitz C, Hesse H, Neumann M, Young AT, et al. Fe valence state of Sr_2FeMoO_6 probed by X-ray absorption spectroscopy: the sample age matters. *J Appl Phys* 2008;**104**:036103.
21. Navarro J, Frontera C, Rubí D, Mestres N, Fontcuberta J. Aging of Sr_2FeMoO_6 and related oxides. *Mater Res Bull* 2003;**38**:1477–86.
22. Retuerto M, Alonso JA, Martínez-Lope MJ, Martínez JL, García-Hernández M. Record saturation magnetization, Curie temperature, and magnetoresistance in Sr_2FeMoO_6 double perovskite synthesized by wet-chemistry techniques. *Appl Phys Lett* 2004;**85**:266–8.
23. Raittila J, Salminem T, Suominem T, Schlesier K, Paturi P. Nanocrystalline Sr_2FeMoO_6 prepared by citrate-gel method. *J Phys Chem Solids* 2006;**67**:1712–8.
24. Sánchez D, García-Hernández M, Auth N, Jakob G. Structural, magnetic, and transport properties of high-quality epitaxial Sr_2FeMoO_6 thin films prepared by pulsed laser deposition. *J Appl Phys* 2004;**96**:2736–42.
25. Zhu XB, Dai JM, Li XH, Zhao BC, Liu SM, Song WH, et al. Chemical solution deposition preparation of double perovskite Sr_2FeMoO_6 film on $LaAlO_3$ (0 0 1) substrate. *Mater Lett* 2005;**59**:2366–9.
26. Colis S, Stoeffer D, Mény C, Fix T, Leuvrey C, Pourroy G, et al. Structural defects in Sr_2FeMoO_6 double perovskite: experimental versus theoretical approach. *J Appl Phys* 2005;**98**:033905.
27. Douy A. Polyacrylamide gel: an efficient tool for easy synthesis of multicomponent oxide precursors of ceramics and glasses. *Int J Inorg Mater* 2001;**3**:699–707.
28. Calleja A, Segarra M, Serradilla IG, Capdevila XG, Fernández AI, Espiell F. Exploring the polyvinyl alcohol method for preparing cuprates and manganites. *J Eur Ceram Soc* 2003;**23**:1369.
29. Rodríguez-Carvajal J. Recent advances in magnetic structure determination by neutron powder diffraction. *Physica B* 1993;**192**:55–69.
30. Bakken E, Støølen S, Norby T, Glenne R, Budd M. Redox energetics of $SrFeO_{3-\delta}$ — a coulometric titration study. *Solid State Ion* 2004;**167**:367–77.
31. Gaskell DR. *Introduction to metallurgical thermodynamics*. New York: McGraw-Hill; 1973. p. 226–227.
32. Savinskaya OA, Nemudry AP, Nadeev AN, Tsybulya SV. Synthesis and study of the thermal stability of $SrFe_{1-x}M_xO_{3-z}$ (M = Mo, W) perovskites. *Solid State Ion* 2008;**179**:1076–9.
33. Veith GM, Greenblatt M, Croft M, Ramanujachary KV, Hattrick-Simpers J, Lofland SE, et al. Synthesis and characterization of $Sr_3FeMoO_{6.88}$: an oxygen-deficient 2D analogue of the double perovskite Sr_2FeMoO_6. *Chem Mater* 2005;**17**:2562–7.
34. Maignan A, Martin C, Hervieu M, Raveau B. Intragrain and intergrain magnetoresistance in Mn, Fe/Mo and Co simple, double and oxygen deficient perovskite oxides. *J Magn Magn Mater* 2000;**211**:173–9.
35. Sakuma H, Ntaniyama T, Kitamoto Y, Yamazaki Y. Cation order and magnetic properties of double perovskite Sr_2FeMoO_6. *J Appl Phys* 2003;**93**:2816–9.